

Actor-Critic Model Predictive Control

Angel Romero, Yunlong Song, Davide Scaramuzza
Robotics and Perception Group
University of Zurich

Abstract: Despite its success, Model Predictive Control (MPC) often requires intensive task-specific engineering and tuning. On the other hand, Reinforcement Learning (RL) architectures minimize this effort, but need extensive data collection and lack interpretability and safety. An open research question is how to combine the advantages of RL and MPC to exploit the best of both worlds. This paper introduces a novel modular RL architecture that bridges these two approaches. By placing a differentiable MPC in the heart of an actor-critic RL agent, the proposed system enables short-term predictions and optimization of actions based on system dynamics, while retaining the end-to-end training benefits and exploratory behavior of an RL agent. The proposed approach effectively handles two different time-horizon scales: short-term decisions managed by the actor MPC and long-term ones managed by the critic network. This provides a promising direction for RL, which combines the advantages of model-based and end-to-end learning methods. We validate the approach in simulated and real-world experiments on a quadcopter platform performing different high-level tasks, and show that the proposed method can learn complex behaviours end-to-end while retaining the properties of an MPC.

1 Introduction

The animal brain’s exceptional ability to quickly learn and adjust to complex behaviors stands out as one of its most remarkable traits, which remains largely unattained by robotic systems. This has often been attributed to the brain’s ability to make both immediate and long-term predictions about the consequences of its actions, and plan accordingly [1, 2, 3]. In the field of robotics and control theory, model-based control has demonstrated a wide array of tasks with commendable reliability [4, 5]. In particular, Model Predictive Control (MPC) has achieved notable success across various domains, including the operation of industrial chemical plants [6], control of legged robots [7], and agile flight with drones [8, 9, 10, 11]. The efficacy of MPC can be attributed to its inherent ability to take actions that optimize for the future states of a system within a defined short time horizon. However, when tasks become exceedingly complex, model-based approaches need considerable effort in hand-engineering the method for each task. This includes hand-crafting the cost function, tuning the hyperparameters, or designing a suitable planning strategy [12, 13]. Furthermore, the modular nature of model-based approaches can lead to the accumulation of errors in a cascading fashion [14, 15, 16].

More recently, end-to-end learning architectures – specifically, Reinforcement Learning (RL) methods – have gained considerable traction due to their ability to alleviate some of these issues [17, 18, 19, 20, 21, 22, 14]. By condensing the engineering effort into reward design, these architectures reduce the per-task design complexity inherent in model-based approaches. Actor-critic methods such as TRPO [23] and PPO [24] have particularly excelled in this domain [25, 26], whereby the agent simultaneously learns an actor policy - a mapping from observation to action - and a critic that aids the learning process by estimating the value function. This value function serves as a measure of the expected rewards to be gathered in a given state, thereby representing the long-term potential of being in a predefined state.

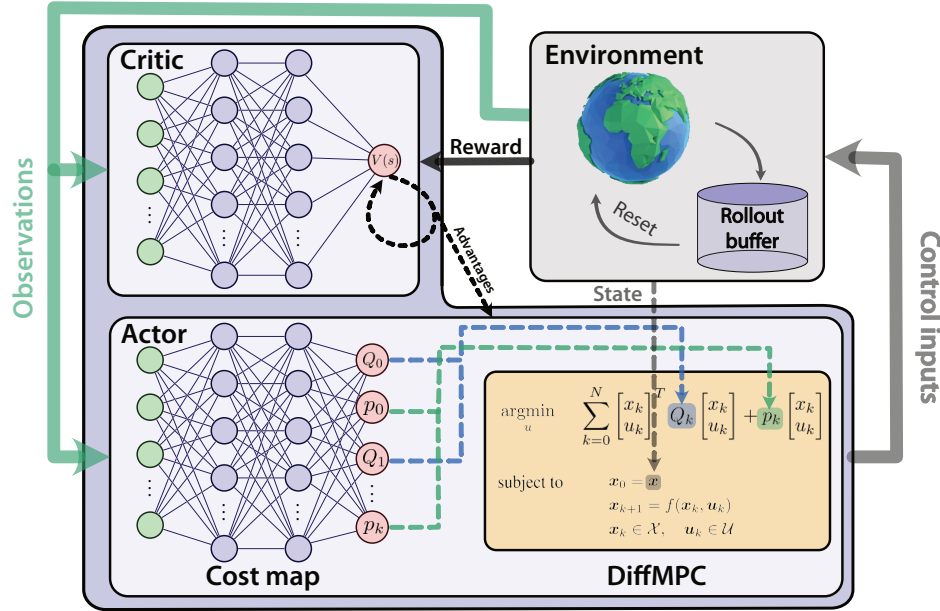


Figure 1: A block diagram of the approach. We combine the strength of actor-critic PPO and the reliability of MPC by placing a differentiable MPC as the last layer of the actor policy. Therefore, at deployment time the commands for the environment are drawn from solving an MPC, which leverages the dynamics of the system and finds the optimal solution given the current state. A neural cost map takes care of mapping the observation space into the cost function space of the MPC. The critic network maps the observations to an approximation of the value function.

However, these architectures are not without their own set of challenges [15, 27]. Training end-to-end without incorporating and leveraging prior knowledge, such as physics or dynamic models, results in need to learn everything from data. While the end-to-end paradigm is attractive, it demands a substantial amount of data and often lacks in terms of interpretability and safety. This has resulted in hesitancy in applying end-to-end learned architectures to safety-critical applications, particularly in cases involving robots that interact with or navigate around humans.

In this paper, we propose a novel approach that addresses these issues by introducing a hybrid actor-critic reinforcement learning architecture. This architecture equips the agent with a differentiable MPC [28], located at the last layer of the actor network, as shown in Fig. 1, that predicts and optimizes the short-term consequences of its actions. The differentiable MPC module, which incorporates a model of the dynamics of the system, provides the agent with prior knowledge even before any training data is received. Moreover, the direct command outputs of the MPC to the environment enhance the safety of the system. The second component of our actor is the cost map – a deep neural network that encapsulates the dependencies between observations and the cost function of the MPC. In other words, while the MPC captures temporal variations inside its horizon, the neural cost module attends to dependencies in relation to the observations. This architecture thereby incorporates two different time horizon scales: the MPC drives the short-term actions while the critic network manages the long-term ones. We demonstrate that the approach can learn complex behaviours – agile flight – for a highly non-linear system – a quadrotor, validated in both simulation and in real-world deployment.

2 Related Work

Several methods have been developed to learn cost functions or dynamic models for MPC [29, 30, 31, 32]. For example, in [31, 32], a policy search strategy is adopted that allows for finding cost function parameters for complex agile flight tasks. However these approaches do not exploit the gradient through the optimization problem, thus not allowing the learned modules to take full advantage of the prior knowledge embedded in the MPC. Recently several approaches that allow for the inclusion of optimization problems in learning pipelines have bloomed [28, 33, 34, 35]. In

particular, the authors in [28] were able to recover the tuning parameters of an MPC via imitation learning for non-linear, low-dimensional dynamics – such as cartpole and inverted pendulum – by backpropagating through the MPC itself. This was enabled by analytically differentiating through the fixed point of a nonlinear iLQR solver [36]. Later, in [37], the authors augment the cost function of a nominal MPC with a learned cost that uses the gradient through the optimizer for the task of navigating around humans. To train this learned cost, they also learn from demonstrations. At the same time, works that aim to make reinforcement learning architectures safer by using MPC have also been on the rise [38, 39]. In [39], a predictive safety filter receives the proposed, end-to-end RL control input and decides if it can be safely applied to the real system, or if it has to be modified otherwise.

3 Methodology

3.1 Preliminaries

Consider the discrete-time dynamic system with continuous state and input spaces, $\mathbf{x}_k \in \mathcal{X}$ and $\mathbf{u}_k \in \mathcal{U}$ respectively. Let us denote the time discretized evolution of the system $f : \mathcal{X} \times \mathcal{U} \mapsto \mathcal{X}$ such that $\mathbf{x}_{k+1} = f(\mathbf{x}_k, \mathbf{u}_k)$, where the sub-index k is used to denote states and inputs at time t_k . The general Optimal Control Problem considers the task of finding a control policy $\pi(\mathbf{x})$, a map from the current state to the optimal input, $\pi : \mathcal{X} \mapsto \mathcal{U}$, such that the cost function $J : \mathcal{X} \mapsto \mathbb{R}^+$ is minimized:

$$\begin{aligned} \pi(\mathbf{x}) = \underset{u}{\operatorname{argmin}} \quad & J(\mathbf{x}) \\ \text{subject to} \quad & \mathbf{x}_0 = \mathbf{x} \\ & \mathbf{x}_{k+1} = f(\mathbf{x}_k, \mathbf{u}_k) \\ & \mathbf{x}_k \in \mathcal{X}, \quad \mathbf{u}_k \in \mathcal{U} \end{aligned} \tag{1}$$

3.2 Trajectory Tracking Model Predictive Control

For standard Model Predictive Control approaches [40, 41, 42], the objective is to minimize a quadratic penalty on the error between the predicted states and inputs, and a given dynamically feasible reference $\mathbf{x}_{k,ref}$ and $\mathbf{u}_{k,ref}$. Consequently, the cost function $J(\mathbf{x})$ in problem (1) is substituted by:

$$J_{MPC}(\mathbf{x}) = \sum_{k=0}^{N-1} \|\Delta \mathbf{x}_k\|_Q^2 + \|\Delta \mathbf{u}_k\|_R^2 + \|\Delta \mathbf{x}_N\|_P^2 \tag{2}$$

where $\Delta \mathbf{x}_k = \mathbf{x}_k - \mathbf{x}_{k,ref}$, $\Delta \mathbf{u}_k = \mathbf{u}_k - \mathbf{u}_{k,ref}$, and where $\mathbf{Q} \succeq 0$, $\mathbf{R} \succ 0$ and $\mathbf{P} \succeq 0$ are the state, input and final state weighting matrices. The norms of the form $\|\cdot\|_A^2$ represent the weighted Euclidean inner product $\|\mathbf{v}\|_A^2 = \mathbf{v}^T \mathbf{A} \mathbf{v}$.

This formulation relies on the fact that a feasible reference $\mathbf{x}_{k,ref}$, $\mathbf{u}_{k,ref}$ is accessible for the future time horizon N . Searching for these is often referred to as *planning*, and for several applications, it becomes rather arduous and computationally expensive [9, 43].

3.3 General Quadratic MPC formulation

Most MPC approaches need an explicit manual selection of a cost function that properly encodes the end task. For the standard tracking MPC presented in the previous section, this encoding is done through planning by finding a dynamically feasible reference trajectory that translates the task into suitable cost function coefficients for every time step. However, this approach presents two drawbacks: i) finding a dense, differentiable cost function – a trajectory – can be difficult, and ii) even if this cost function is found, extra effort needs to be spent in fine tuning the parameters for real-world deployment. More generally, all receding horizon architectures such as MPC need to run in real-time when a deployment in the real world is desired. Because of this, the optimization

problem is often approximated and converted from a non-linear optimization problem to a Quadratic Program (QP). Therefore, a task agnostic cost function can be written (3).

$$J_Q(\mathbf{x}) = \sum_{k=0}^N \begin{bmatrix} x_k \\ u_k \end{bmatrix}^T Q_k \begin{bmatrix} x_k \\ u_k \end{bmatrix} + p_k \begin{bmatrix} x_k \\ u_k \end{bmatrix} \quad (3)$$

In our paper we propose to directly search for the matrix coefficients of (3). This way, by varying Q_k and p_k , we are able capture a larger family of problems, without suffering from the dependency on a feasible trajectory.

3.4 Actor-Critic Model Predictive Control

In this paper we propose an Actor Critic MPC controller architecture where the MPC is differentiable and the cost function is learned end-to-end using RL. The MPC block is introduced as the final layer of the actor in an actor-critic PPO pipeline, as shown in Fig. 1. Instead of resorting to task specific engineering of the cost function, we propose a neural cost map where the Q_k and p_k terms are the output of a neural network. This allows to encode the end task directly as a reward function, which is then trainable end-to-end using the PPO training scheme. The main benefit of this approach with respect to training a pure Multi Layer Perceptron (MLP) end-to-end is that the final layer of the actor is a model-based MPC controller, and therefore it retains its reliability and interpretability properties. The model-based controller in the final layer ensures that the commands are always feasible for the dynamics at hand, and that they respect the system constraints. To allow for exploration, during training the control outputs are sampled from a Gaussian distribution where the mean is the output of the MPC block, and the variance is controlled by the PPO algorithm. However, during deployment the output from the MPC is used directly on the system, retaining all properties of a model-based controller.

3.5 Neural Cost Map

The cost function for the model predictive control architecture presented in Section 3.4 is learnt as a neural network, depicted in Fig. 1 as *Cost Map*. Several adaptations to the system are needed in order to properly interface the neural network architecture with the optimization problem. First, we constrain the Q_k matrix to be diagonal.

$$Q_k = \text{diag}(Q_{x_1,k}, \dots, R_{u_1,k}, \dots) \quad p_k = [p_{x_1,k}, \dots, p_{u_1,k}, \dots] \quad \forall k \in 0, \dots, T \quad (4)$$

where x_1, \dots and u_1, \dots are the states and inputs to the system, respectively, and $Q_{x_1,k}$ and $p_{x_1,k}$ are the learnable parameters, interface from the neural network to the optimization problem.

The purpose of the diagonalization of the Q matrix is to reduce the dimensionality of the learnable parameter space. Therefore, the dimensionality of the output dimension of this *Cost Map* is $2T(n_{state} + n_{input})$. In order to ensure the positive semi-definiteness of the Q matrix and the positive definiteness of the R matrix, a lower bound on the value that these coefficients needs to be set. To this end, the last layer of the neural cost map has been chosen to be a sigmoid which allows for upper and lower bounds on the output value. This lower and upper limits are chosen equal for Q and p, of 0.1 and 100000.0, respectively. The upper bound is needed because otherwise a behaviour where the coefficients would grow to infinity is observed. Therefore, the final neural cost map consists of two hidden layers of width 512 with ReLUs in between and a sigmoid non-linearity at the end. The critic network consists also of two hidden layers of width 512 and ReLUs. The output of the critic network is a scalar.

4 Experiments

In this section we present a set of experiments, both in simulation and in the real-world. All experiments have been conducted using a quadrotor platform. We train in a simple simulator in order to speed up the training, and evaluate in BEM, a high-fidelity simulator [44], which is slower but has a higher level of similarity with the real-world. The dynamics of the quadrotor platform are

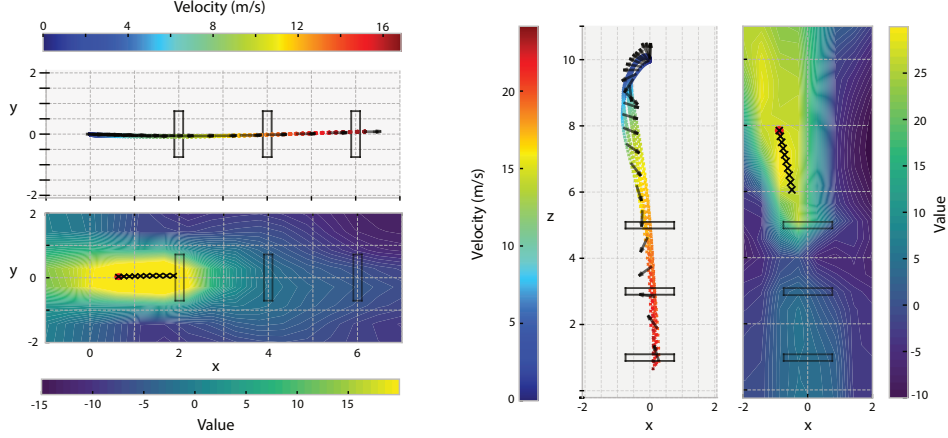


Figure 2: Actor-Critic Model Predictive Control (MPC) applied to agile flight through gates: Velocity profiles and corresponding value function plots. The left side illustrates horizontal flight, while the right side shows vertical flight. In the value function plots, areas with high values (depicted in yellow) indicate regions with the highest expected rewards. The MPC predictions demonstrate a clear preference for regions of high value, emphasizing the model’s focus on long-term predictions captured by the value function, in contrast to the short-term predictions of the model-predictive controller.

introduced in supplementary Section 7.1. First, in Section 4.1 we present a series of simulation experiments and ablation studies on two standard tracks: Horizontal and Vertical. Then, in Section 4.2 we showcase the ability of our approach to learn more complex agile flight behaviours. Next, in Section 4.3 we show that the proposed method is also able to learn perception aware flight. Finally, we show that our approach transfers to the real world in Section 4.4. For every different task the policies are retrained from scratch. For these experiments, the observation space consists of linear velocity, rotation matrix and relative measurement of the target gate’s corners. The control input modality is collective thrust and body rates. Even if the MPC block uses a model which limits the actuation at the single rotor thrust level, collective thrust and body rates are computed from these and applied to the system. This ensures that the computed inputs are feasible for the model of the platform. Finally, the reward function depends on the task. One common term that is shared among all tasks in our set of experiments is the *progress reward*, which incentivizes the platform to fly as fast as possible to a goal. For more details about the rewards, observations and dynamics we refer the reader to supplementary Section 7.3.

4.1 Horizontal and Vertical tracks

We start with horizontal and vertical flight. These tasks were chosen because they expose the fundamental capabilities of our system, are basic enough to allow for fast iteration cycles, and therefore are taken as base for the main ablation studies presented in this section. For example, the vertical task can show if the approach is able to find a solution that lies directly in the singularity of the input space of the platform, since the platform can only generate thrust in its positive body Z direction. When flying fast downwards, the fastest solution is to tilt the drone as soon as possible, direct the thrust downwards and only then command positive thrust [9]. However, there is a local optimum where many approaches are prone to get stuck [12], which is command zero thrust and wait to be pulled only by the force of gravity. Fig. 2 shows the simulation results of deploying the proposed approach which was trained in the horizontal and vertical tracks (left and right side of Fig. 2, respectively). In this figure we show velocity profiles and value function profiles. The value function profiles have been computed by selecting a state of the platform in the trajectory and modifying only the position while keeping the rest of the states fixed. For the horizontal track we sweep only the XY positions, and for the vertical track, the XZ positions. Additionally, 10 MPC predictions are shown and marked with Xs. In these value function plots, areas with high values (in yellow) indicate regions with high expected rewards. This experiment shows that the proposed approach can

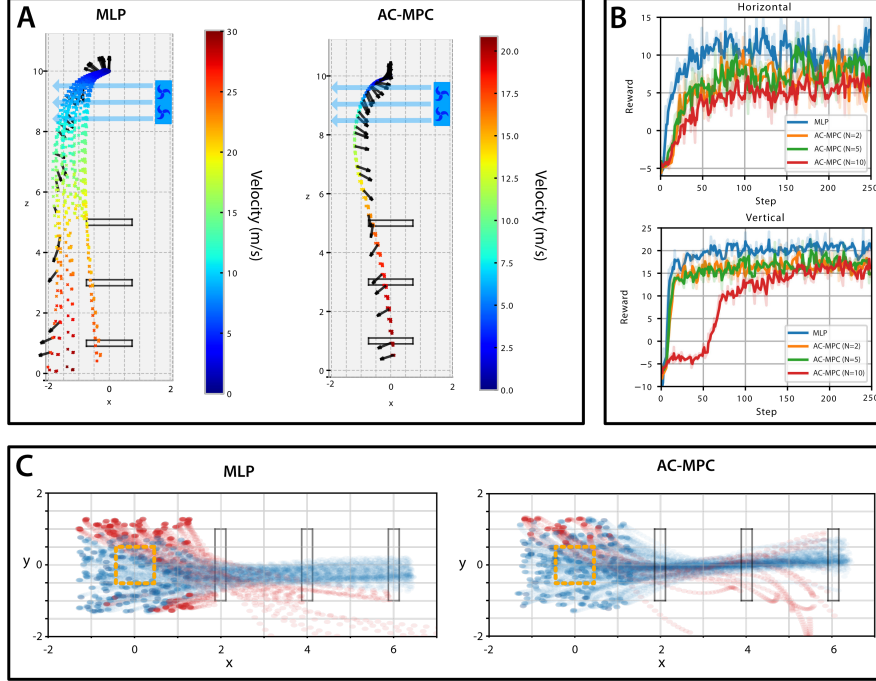


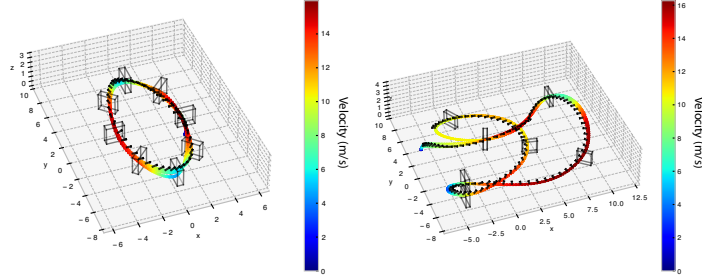
Figure 3: A: a comparison of a pure MLP and our AC-MPC approach when facing unknown disturbances. In this case, a constant wind force of 11.5 N is acting on the platform. The policies have been trained without disturbances. B: depicts the reward evolution for our approach compared to MLP, considering various horizon lengths, for both Vertical and Horizontal tasks. C: an ablation study on the trained policies’ robustness to changes in initial conditions for the horizontal flight task. Trajectories are color-coded, with red indicating crashed trajectories and blue denoting successful ones. The policies were trained with randomized initial conditions, visually marked within a yellow rectangle.

not only successfully recover an effective policy for the task, but it is also able to exploit the benefits of both MPC and RL approaches. The critic has indeed been able to learn long term predictions, while the model-predictive controller focuses on the short term ones, effectively incorporating two time scales. In the attached supplementary video we also show how these high value areas evolve as the platform flies towards the end of the track.

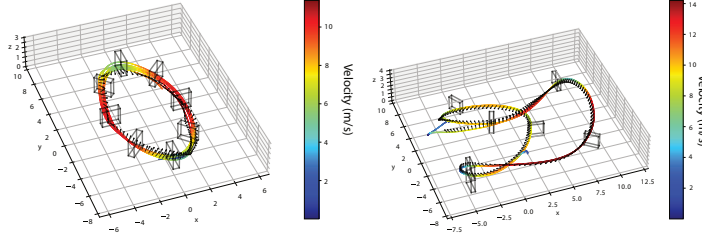
4.1.1 Ablation study: sample efficiency and robustness to disturbances

In order to understand the properties of the proposed method, we perform two studies where the pure MLP architecture (labeled as *MLP* in the following) is compared to our approach (labeled as *AC-MPC*) in terms of sample efficiency and robustness to disturbances. All approaches have been trained with exactly the same conditions (reward, environment, observation, etc), the only change being the policy itself. As shown in Fig. 3B, in terms of sample efficiency, for both the horizontal and the vertical flight tasks our approach falls slightly behind. This can be due to the fact that by using an MPC architecture we are imposing certain rigid dynamic structure when compared to using only an MLP. This is supported by the fact that, as depicted in Fig. 3B, the sample efficiency gets worse with the horizon length, as the number of cost function parameters grows linearly with the horizon.

In terms of disturbance rejection, we conduct two extra ablations (Fig. 3A and Fig. 3C) where we test how both approaches react when presented with situations outside the training distribution, and therefore, test for generalisability and reliability. In Fig. 3A, we simulate a strong wind gust that applies a constant external force of 11.5 N (equivalent to 1.5x the weight of the platform). This force is applied when the drone flies from 10m to 8m in height. We can see how the pure MLP policy is not able to recover and go back to the designated track. On the other hand, AC-MPC is able to



(a) Simulation results



(b) Real-world results

Figure 4: Actor-Critic MPC trained for the task of agile flight in complex environments. On the left Circle track and on the right, SplitS track, for both real world and simulation. These figures show how our approach is able to be deployed in the real world and how they transfer zero shot from simulation to reality.

recover properly, while at the same time being more consistent. This showcases that incorporating a model-based component enables the system to achieve improved robustness and reliability.

In the case of Fig. 3C, we simulate 10000 iterations for each controller for the horizontal task, where the starting point is uniformly sampled in a cube of 3m of side length where the nominal starting point is in the center. During training, the initial position is only randomized in a cube of 1m of side length (shown in yellow in Fig. 3). The successful trajectories are shown in blue, while the crashed ones are shown in red. We can observe that the AC-MPC presents higher success rate, and that it is more consistent (indicated by the dark blue area in the center of the gates). Both experiments support the claim that AC-MPC deals better with unforeseen situations and unknown disturbances, which makes it less fragile and more generalisable.

4.2 Complex tracks: Circle and SplitS

To showcase the capability of the proposed method being able to learn agile flight through complex environments, in this section we focus on two extra environments: *Circle* and *SplitS*. Fig. 4a shows how the approach is able to learn agile flight through these two tracks, with maximum speeds of up to 16 m/s in simulation.

4.3 Perception Aware Flight

Additionally, we create a training environment where the task is to fly agilely in a circle while keeping a certain point in the center of the camera frame. This approach is similar to the one in [45]. However in this case the perception aware objective is in the form of a reward function instead of an optimization objective. Given an interest point in the world frame (which is marked as an orange star in Fig. 5), we minimize the angle between the Z-axis of the camera and the line that joins the center point of the camera with the objective. This reward term is then summed to the previously presented progress reward term, which incentivizes the drone to move through the gates. In Fig. 5 we show how both MLP and AC-MPC approaches are able to learn this behaviour. In this case the black arrows represent the direction of the camera Z-axis. Since yaw control effectiveness is the

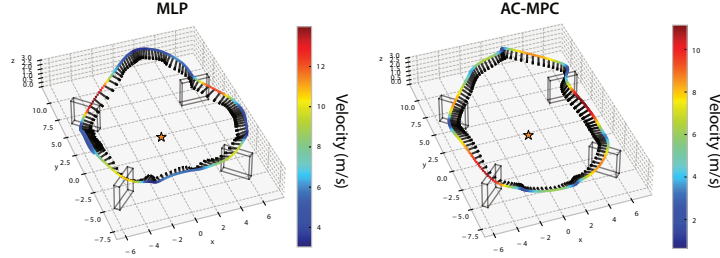


Figure 5: The proposed Actor-Critic Model Predictive Controller trained for the task of agile perception aware flight. The star in the middle of the track is the point to be kept in the middle of the camera frame.

lowest for a quadrotor – a large amount of actuation is needed for a small change in yaw –, this task poses a competing reward problem, where if the drone moves faster, it will be necessarily at the expense of losing perception awareness. This is the reason behind the unnatural shapes that emerge from the training, shown in Fig. 5.

4.4 Real-world transfer

In this section we show that the proposed approach is able to transfer zero shot to the real world. To show it we deploy the policy the tracks introduced in Section 4.2: Circle track and SplitS track. For the real-world deployment we use the Agilicious platform [46]. The main physical parameters and components of this platform have been described in supplementary Section 7.2. In Fig. 4b highlight the strong similarities between the simulated and the real world experiments, which indicates that the approach presents very good zero-shot transfer properties. These experiments are also shown in the supplementary video.

5 Limitations

In this paper, we introduce the AC-MPC approach, which can leverage the advantages of both MPC and RL. However, there are some limitations to be mentioned and to be improved in the future. First, training with the MPC in the loop takes significantly longer than its only MLP counterpart. As shown in supplementary Section 7.4, while an MLP policy takes 21 minutes of training in a GPU, for the same number of timesteps our policy takes 11 hours for $N=2$, or 39 hours for $N=10$ in a CPU. The main reason behind this is that for every differentiable MPC backward or forward pass, an optimization problem needs to be solved. This limitation can be alleviated by implementing the controller and the solver in C++, since right now our entire pipeline is implemented in python. In fact, there are open-source libraries [33, 34] that are recently evolving and implementing the differentiable MPC block in C++. Another limitation is that the differentiable MPC controller does not support one important characteristic of model based control: state constraints. In order to ensure safety we often need to limit the states that can be visited by our system (e.g., limitations in speeds or body rates). This limitation could be addressed by exploring the possibilities of adding state constraints to the implementation.

6 Conclusion and Discussion

In this work we present a hybrid PPO actor-critic based agent that contains a differentiable model predictive controller at its core. We show that not only is the method able to learn complex behaviours for a highly non-linear and high dimensional system such a quadrotor, but that it also improves over its MLP counterpart in terms of generalisability and reliability. Additionally, our approach is able to transfer zero-shot to the real world. This capability is demonstrated by successfully piloting a quadrotor at velocities of up to 14 m/s, without prior specific training for the real-world setting. We believe that the proposed method represents an important step in the direction of interpretability and safety in RL and demonstrates that modular solutions that combine the best of learning-centric and model-based approaches are becoming increasingly promising. Our approach potentially paves the way for the development of more reliable, efficient, and safe RL-based systems, contributing positively towards the broader goal of advancing AI and robotics applications.

Acknowledgments

This work was supported by the Swiss National Science Foundation (SNSF) through the National Centre of Competence in Research (NCCR) Robotics (grant number 51NF40 185543), the European Union’s Horizon 2020 Research and Innovation Programme under grant agreement No. 871479 (AERIAL-CORE), and the European Research Council (ERC) under grant agreement No. 864042 (AGILEFLIGHT). We would also like to thank Brandon Amos, for sharing his insights regarding the implementation of the differentiable MPC code, and Jiaxu Xing for the insightful discussions.

References

- [1] R. P. N. Rao and D. H. Ballard. Predictive coding in the visual cortex: a functional interpretation of some extra-classical receptive-field effects. *Nature Neuroscience*, 2(1):79–87, 1999. ISSN 1546-1726. doi:10.1038/4580. URL <https://doi.org/10.1038/4580>.
- [2] K. Friston. The free-energy principle: a unified brain theory? *Nature Reviews Neuroscience*, 11(2):127–138, 2010. ISSN 1471-0048. doi:10.1038/nrn2787. URL <https://doi.org/10.1038/nrn2787>.
- [3] Y. LeCun. A path towards autonomous machine intelligence version 0.9. 2, 2022-06-27. *Open Review*, 62, 2022.
- [4] T. Tzanetos, M. Aung, J. Balaram, H. F. Grip, J. T. Karras, T. K. Canham, G. Kubiak, J. Anderson, G. Merewether, M. Starch, M. Pauken, S. Cappucci, M. Chase, M. Golombek, O. Toupet, M. C. Smart, S. Dawson, E. B. Ramirez, J. Lam, R. Stern, N. Chahat, J. Ravich, R. Hogg, B. Pipenberg, M. Keennon, and K. H. Williford. Ingenuity mars helicopter: From technology demonstration to extraterrestrial scout. In *2022 IEEE Aerospace Conference (AERO)*, pages 01–19. IEEE, 2022. doi:10.1109/AERO53065.2022.9843428.
- [5] E. Arthur Jr and J.-C. Ho. *Applied optimal control: optimization, estimation, and control*. Hemisphere, 1975.
- [6] M. Ellis, J. Liu, and P. D. Christofides. *Economic Model Predictive Control: Theory, Formulations and Chemical Process Applications*. Springer, 2016.
- [7] P.-B. Wieber, R. Tedrake, and S. Kuindersma. Modeling and control of legged robots. In *Springer handbook of robotics*, pages 1203–1234. Springer, 2016.
- [8] P. Foehn, D. Brescianini, E. Kaufmann, T. Cieslewski, M. Gehrig, M. Muglikar, and D. Scaramuzza. Alphapilot: Autonomous drone racing. *Robotics: Science and Systems (RSS)*, 2020.
- [9] P. Foehn, A. Romero, and D. Scaramuzza. Time-optimal planning for quadrotor waypoint flight. *Science Robotics*, 6(56), 2021. doi:10.1126/scirobotics.abh1221. URL <https://robotics.sciencemag.org/content/6/56/eabh1221>.
- [10] A. Romero, S. Sun, P. Foehn, and D. Scaramuzza. Model predictive contouring control for time-optimal quadrotor flight. *IEEE Transactions on Robotics*, pages 1–17, 2022. doi:10.1109/TRO.2022.3173711.
- [11] A. Romero, R. Penicka, and D. Scaramuzza. Time-optimal online replanning for agile quadrotor flight. *IEEE Robotics and Automation Letters*, 7(3):7730–7737, 2022. doi:10.1109/LRA.2022.3185772.
- [12] A. Romero, S. Sun, P. Foehn, and D. Scaramuzza. Model predictive contouring control for time-optimal quadrotor flight. *IEEE Transactions on Robotics*, 38(6):3340–3356, 2022.
- [13] D. V. Lu, D. Hershberger, and W. D. Smart. Layered costmaps for context-sensitive navigation. In *2014 IEEE/RSJ International Conference on Intelligent Robots and Systems*, pages 709–715, 2014. doi:10.1109/IROS.2014.6942636.
- [14] Y. Song, A. Romero, M. Mueller, V. Koltun, and D. Scaramuzza. Reaching the limit in autonomous racing: Optimal control versus reinforcement learning. *Science Robotics*, 2023.
- [15] N. Roy, I. Posner, T. D. Barfoot, P. Beaudoin, Y. Bengio, J. Bohg, O. Brock, I. Depatie, D. Fox, D. E. Koditschek, T. Lozano-Perez, V. K. Mansinghka, C. J. Pal, B. A. Richards, D. Sadigh, S. Schaal, G. S. Sukhatme, D. Thérien, M. Toussaint, and M. van de Panne. From machine learning to robotics: Challenges and opportunities for embodied intelligence. *ArXiv*, abs/2110.15245, 2021.

- [16] X. Xiao, B. Liu, G. Warnell, and P. Stone. Motion planning and control for mobile robot navigation using machine learning: a survey. *Autonomous Robots*, 46(5):569–597, 2022.
- [17] D. Silver, A. Huang, C. Maddison, A. Guez, L. Sifre, G. van den Driessche, J. Schrittwieser, I. Antonoglou, V. Panneershelvam, M. Lanctot, et al. Mastering the game of go with deep neural networks and tree search. *Nature*, 529(7587):484–489, 2016.
- [18] O. Vinyals, I. Babuschkin, W. Czarnecki, M. Mathieu, A. Dudzik, J. Chung, D. Choi, R. Powell, T. Ewalds, P. Georgiev, et al. Grandmaster level in starcraft ii using multi-agent reinforcement learning. *Nature*, 575(7782):350–354, 2019.
- [19] J. Degraeve, F. Felici, J. Buchli, M. Neunert, B. Tracey, F. Carpanese, T. Ewalds, R. Hafner, A. Abdolmaleki, D. de las Casas, C. Donner, L. Fritz, C. Galperti, A. Huber, J. Keeling, M. Tsimpoukelli, J. Kay, A. Merle, J.-M. Moret, S. Noury, F. Pesamosca, D. Pfau, O. Sauter, C. Sommariva, S. Coda, B. Duval, A. Fasoli, P. Kohli, K. Kavukcuoglu, D. Hassabis, and M. Riedmiller. Magnetic control of tokamak plasmas through deep reinforcement learning. *Nature*, 602:414–419, 2022. doi:[10.1038/s41586-021-04301-9](https://doi.org/10.1038/s41586-021-04301-9).
- [20] D. Mankowitz, A. Michi, A. Zhernov, et al. Faster sorting algorithms discovered using deep reinforcement learning. *Nature*, 618:257–263, 2023. URL <https://doi.org/10.1038/s41586-023-06004-9>.
- [21] J. Lee, J. Hwangbo, L. Wellhausen, V. Koltun, and M. Hutter. Learning quadrupedal locomotion over challenging terrain. *Science robotics*, 5(47):eabc5986, 2020.
- [22] T. Miki, J. Lee, J. Hwangbo, L. Wellhausen, V. Koltun, and M. Hutter. Learning robust perceptive locomotion for quadrupedal robots in the wild. *Science Robotics*, 7(62):eabk2822, 2022.
- [23] J. Schulman, S. Levine, P. Abbeel, M. Jordan, and P. Moritz. Trust region policy optimization. In *International conference on machine learning*, pages 1889–1897. PMLR, 2015.
- [24] J. Schulman, F. Wolski, P. Dhariwal, A. Radford, and O. Klimov. Proximal policy optimization algorithms. *arXiv e-prints*, 2017.
- [25] V. Mnih, K. Kavukcuoglu, D. Silver, A. A. Rusu, J. Veness, M. G. Bellemare, A. Graves, M. Riedmiller, A. K. Fidjeland, G. Ostrovski, et al. Human-level control through deep reinforcement learning. *nature*, 518(7540):529–533, 2015.
- [26] D. Silver, A. Huang, C. J. Maddison, A. Guez, L. Sifre, G. Van Den Driessche, J. Schrittwieser, I. Antonoglou, V. Panneershelvam, M. Lanctot, et al. Mastering the game of go with deep neural networks and tree search. *nature*, 529(7587):484–489, 2016.
- [27] L. Brunke, M. Greeff, A. W. Hall, Z. Yuan, S. Zhou, J. Panerati, and A. P. Schoellig. Safe learning in robotics: From learning-based control to safe reinforcement learning. *Annual Review of Control, Robotics, and Autonomous Systems*, 5:411–444, 2022.
- [28] B. Amos, I. Jimenez, J. Sacks, B. Boots, and J. Z. Kolter. Differentiable mpc for end-to-end planning and control. *Advances in neural information processing systems*, 31, 2018.
- [29] A. Saviolo, G. Li, and G. Loianno. Physics-inspired temporal learning of quadrotor dynamics for accurate model predictive trajectory tracking. *IEEE Robotics and Automation Letters*, 7(4): 10256–10263, 2022.
- [30] G. Torrente, E. Kaufmann, P. Föhn, and D. Scaramuzza. Data-driven mpc for quadrotors. *IEEE Robotics and Automation Letters*, 6(2):3769–3776, 2021. doi:[10.1109/LRA.2021.3061307](https://doi.org/10.1109/LRA.2021.3061307).
- [31] A. Romero, S. Govil, G. Yilmaz, Y. Song, and D. Scaramuzza. Weighted maximum likelihood for controller tuning. *ArXiv*, abs/2210.11087, 2022.

- [32] Y. Song and D. Scaramuzza. Policy search for model predictive control with application to agile drone flight. *IEEE Transactions on Robotics*, 38(4):2114–2130, 2022.
- [33] L. Pineda, T. Fan, M. Monge, S. Venkataraman, P. Sodhi, R. T. Chen, J. Ortiz, D. DeTone, A. Wang, S. Anderson, J. Dong, B. Amos, and M. Mukadam. Theseus: A Library for Differentiable Nonlinear Optimization. *Advances in Neural Information Processing Systems*, 2022.
- [34] C. Wang, D. Gao, K. Xu, J. Geng, Y. Hu, Y. Qiu, B. Li, F. Yang, B. Moon, A. Pandey, Aryan, J. Xu, T. Wu, H. He, D. Huang, Z. Ren, S. Zhao, T. Fu, P. Reddy, X. Lin, W. Wang, J. Shi, R. Talak, K. Cao, Y. Du, H. Wang, H. Yu, S. Wang, S. Chen, A. Kashyap, R. Bandaru, K. Dantu, J. Wu, L. Xie, L. Carlone, M. Hutter, and S. Scherer. PyPose: A library for robot learning with physics-based optimization. In *IEEE/CVF Conference on Computer Vision and Pattern Recognition (CVPR)*, 2023.
- [35] S. East, M. Gallieri, J. Masci, J. Koutnik, and M. Cannon. Infinite-horizon differentiable model predictive control. *arXiv preprint arXiv:2001.02244*, 2020.
- [36] W. Li and E. Todorov. Iterative linear quadratic regulator design for nonlinear biological movement systems. In *ICINCO (1)*, pages 222–229. Citeseer, 2004.
- [37] X. Xiao, T. Zhang, K. M. Choromanski, T.-W. E. Lee, A. Francis, J. Varley, S. Tu, S. Singh, P. Xu, F. Xia, S. M. Persson, D. Kalashnikov, L. Takayama, R. Frostig, J. Tan, C. Parada, and V. Sindhwani. Learning model predictive controllers with real-time attention for real-world navigation. In *CoRL*, 2022. URL <https://openreview.net/forum?id=7Nwds2LjN1s>.
- [38] M. Zanon and S. Gros. Safe reinforcement learning using robust mpc. *IEEE Transactions on Automatic Control*, 66(8):3638–3652, 2020.
- [39] K. P. Wabersich and M. N. Zeilinger. A predictive safety filter for learning-based control of constrained nonlinear dynamical systems. *Automatica*, 129:109597, 2021. ISSN 0005-1098. doi:<https://doi.org/10.1016/j.automatica.2021.109597>. URL <https://www.sciencedirect.com/science/article/pii/S0005109821001175>.
- [40] H. Nguyen, M. Kamel, K. Alexis, and R. Siegwart. Model predictive control for micro aerial vehicles: A survey. *2021 European Control Conference (ECC)*, 2021. doi:10.23919/ecc54610.2021.9654841.
- [41] M. Bangura and R. Mahony. Real-time model predictive control for quadrotors. *IFAC World Congress*, 2014. doi:10.3182/20140824-6-za-1003.00203.
- [42] M. Diehl, H. G. Bock, H. Diedam, and P. B. Wieber. Fast direct multiple shooting algorithms for optimal robot control. In *Fast motions in biomechanics and robotics*. Springer, 2006.
- [43] Y. Song, M. Steinweg, E. Kaufmann, and D. Scaramuzza. Autonomous drone racing with deep reinforcement learning. *2021 IEEE/RSJ International Conference on Intelligent Robots and Systems (IROS)*, 2021. doi:10.1109/IROS51168.2021.9636053.
- [44] L. Bauersfeld, E. Kaufmann, P. Foehn, S. Sun, and D. Scaramuzza. Neurobem: Hybrid aerodynamic quadrotor model. *Proceedings of Robotics: Science and Systems XVII*, page 42, 2021.
- [45] D. Falanga, P. Foehn, P. Lu, and D. Scaramuzza. Pampe: Perception-aware model predictive control for quadrotors. In *2018 IEEE/RSJ International Conference on Intelligent Robots and Systems (IROS)*, pages 1–8. IEEE, 2018.
- [46] P. Foehn, E. Kaufmann, A. Romero, R. Penicka, S. Sun, L. Bauersfeld, T. Laengle, G. Cioffi, Y. Song, A. Loquercio, and D. Scaramuzza. Agilicious: Open-source and open-hardware agile quadrotor for vision-based flight. *Science Robotics*, 7(67):eabl6259, 2022. doi:10.1126/scirobotics.abl6259. URL <https://www.science.org/doi/abs/10.1126/scirobotics.abl6259>.

7 Supplementary Material

7.1 Drone dynamics

The quadrotor's state space is described from the inertial frame I to the body frame B , as $\mathbf{x} = [\mathbf{p}_{IB}, \mathbf{q}_{IB}, \mathbf{v}_{IB}, \boldsymbol{\omega}_B]^T$ where $\mathbf{p}_{IB} \in \mathbb{R}^3$ is the position, $\mathbf{q}_{IB} \in \mathbb{SO}(3)$ is the unit quaternion that describes the rotation of the platform, $\mathbf{v}_{IB} \in \mathbb{R}^3$ is the linear velocity vector, and $\boldsymbol{\omega}_B \in \mathbb{R}^3$ are the bodyrates in the body frame. The input of the system is given as the collective thrust $\mathbf{f}_B = [0 \ 0 \ f_{Bz}]^T$ and body torques $\boldsymbol{\tau}_B$. For readability, we drop the frame indices as they are consistent throughout the description. The dynamic equations are

$$\begin{aligned} \dot{\mathbf{p}} &= \mathbf{v} & \dot{\mathbf{q}} &= \frac{1}{2} \mathbf{q} \odot \begin{bmatrix} 0 \\ \boldsymbol{\omega} \end{bmatrix} \\ \dot{\mathbf{v}} &= \mathbf{g} + \frac{1}{m} \mathbf{R}(\mathbf{q}) \mathbf{f}_T & \dot{\boldsymbol{\omega}} &= \mathbf{J}^{-1} (\boldsymbol{\tau} - \boldsymbol{\omega} \times \mathbf{J} \boldsymbol{\omega}) \end{aligned} \quad (5)$$

where \odot represents the Hamilton quaternion multiplication, $\mathbf{R}(\mathbf{q})$ the quaternion rotation, m the quadrotor's mass, and \mathbf{J} the quadrotor's inertia.

Additionally, the input space given by \mathbf{f} and $\boldsymbol{\tau}$ is decomposed into single rotor thrusts $\mathbf{f} = [f_1, f_2, f_3, f_4]$ where f_i is the thrust at rotor $i \in \{1, 2, 3, 4\}$.

$$\mathbf{f}_T = \begin{bmatrix} 0 \\ 0 \\ \sum f_i \end{bmatrix} \quad \text{and} \quad \boldsymbol{\tau} = \begin{bmatrix} l/\sqrt{2}(f_1 + f_2 - f_3 - f_4) \\ l/\sqrt{2}(-f_1 + f_2 + f_3 - f_4) \\ c_\tau(f_1 - f_2 + f_3 - f_4) \end{bmatrix} \quad (6)$$

with the quadrotor's arm length l and the rotor's torque constant c_τ .

7.2 Quadrotor parameters

In this section we introduce the quadrotor parameters that are used for the real world experiments. The details about components and physical parameters can be seen in Table 1.

7.3 Observations, control inputs and rewards

In this section we introduce the observation space, the control input space and the rewards used for each task.

7.3.1 Observations

For all tasks presented in our manuscript, the observation space does not change, and it consists of two main parts: the vehicle observation $\mathbf{o}_t^{\text{quad}}$ and the race track observation $\mathbf{o}_t^{\text{track}}$. We define the vehicle state as $\mathbf{o}_t^{\text{quad}} = [\mathbf{v}_t, \mathbf{R}_t] \in \mathbb{R}^{12}$, which corresponds to the quadrotor's linear velocity and rotation matrix. We define the track observation vector as $\mathbf{o}_t^{\text{track}} = [\delta \mathbf{p}_1, \dots, \delta \mathbf{p}_i, \dots]$, $i \in [1, \dots, N]$, where $\delta \mathbf{p}_i \in \mathbb{R}^{12}$ denotes the relative position between the vehicle center and the four corners of the next target gate i or the relative difference in corner distance between two consecutive gates. Here $N \in \mathbb{Z}^+$ represents the total number of future gates. This formulation of the track observation allows us to incorporate an arbitrary number of future gates into the observation. We use $N = 2$, meaning we observe the four corners of the next two target gates. We normalize the observation by calculating the mean and standard deviation of the input observations at each training iteration.

7.3.2 Control inputs

The control inputs are expressed as a 4-dimensional vector $\mathbf{a} = [c, \omega_x, \omega_y, \omega_z] \in \mathbb{R}^4$, representing mass-normalized collective thrust and bodyrates, in each axis separately. Since our differentiable MPC block outputs single rotor thrusts, we obtain the mass-normalized collective thrust as $\sum f_i/m$. For the body rates, we take the first prediction of the differentiable MPC as input for our system. This

Agilicious platform



Parameters	Agilicious platform
Thrust-to-weight Ratio	4.62
Mass [kg]	0.75
Maximum Thrust [N]	34.00
Arm Length [m]	0.15
Inertia [g m ²]	[2.50, 2.51, 4.32]
Motor Time Constant [s]	0.033
Components	Agilicious platform
Frame	Chameleon 6 inch
Motor	Xrotor 2306
Propeller	Azure Power SFP 5148 5
Flight Controller	BrainFPV radix
Battery	Tattu 4 cells 1800 mAh
Electronic Speed Controller (ESC)	Hobbywing XRotor

Table 1: **Overview of the drone parameters for real-world experiments.** The 4s Drone is used for the baseline comparison between our RL policy and optimal control methods.

way, all inputs sent to the system are ensured to fulfill the single rotor thrust constraints enforced by the MPC.

7.3.3 Rewards

Throughout this work different reward terms have been used depending on the task. For all the experiments there is one reward term in common, which is the gate progress reward. This term encourages the platform to fly as fast as possible. Additionally, for the perception aware task one more term has been added. Both terms are explained in what follows.

Gate Progress term

The objective is to directly maximize progress toward the center of the next gate. Once the current gate is passed, the target gate switches to the next one. At each simulation time step k , the gate progress objective is defined

$$r(k) = \|g_k - p_{k-1}\| - \|g_k - p_k\| - b\|\omega_k\| \quad (7)$$

where g_k represents the target gate center, and p_k and p_{k-1} are the vehicle positions at the current and previous time steps, respectively. Here, $b\|\omega_k\|$ is a penalty on the bodyrate multiplied by a coefficient $b = 0.01$. To discourage collisions with the environment, a penalty ($r(k) = -10.0$) is imposed when the vehicle experiences a collision. The agent is rewarded with a positive reward ($r(k) = +10.0$) upon finishing the race.

Perception Aware term

Let us assume that we mount a camera to the frame of the drone. The perception aware task is defined as keeping the Z-axis of the camera always pointing towards the point of interest. Let us define the unit vector associated to this Z-axis as \mathbf{z}_c . Let us denote the position of the interest point as \mathbf{p}_i , and the position of the center of the camera frame as \mathbf{p}_c . Therefore, the vector from the center of the camera frame and the point of interest is $\mathbf{r}_{ci} = \mathbf{p}_i - \mathbf{p}_c$, and its normalized version is \mathbf{u}_{ci} . Therefore, the angle between \mathbf{z}_c and \mathbf{u}_{ci} is $\alpha = \arccos(\mathbf{z}_c \cdot \mathbf{u}_{ci})$. We are interested in giving positive rewards when this angle is close to zero, for which we use $r_{pa}(k) = \exp(-5\alpha_k^4)$, shown in Fig. 6.

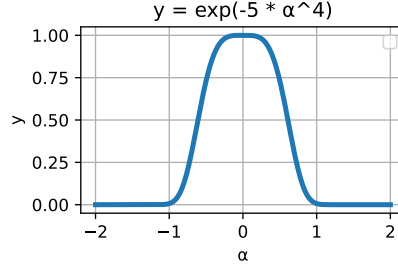


Figure 6: Perception aware reward. The function shows that we give high rewards for the α angle being close to zero.

7.4 Training time and forward pass time

In Table 2 we show the training times and the forward pass times for the MLP approach, as well as for our proposed AC-MPC approach for different horizon lengths.

Table 2: Model Performance				
	MLP	AC-MPC (N=2)	AC-MPC (N=5)	AC-MPC (N=10)
Training time	21m	11h30m	22h6m	39h36m
Forward time	0.5 ± 0.037 ms	13.5 ± 1.1 ms	37.5 ± 14.5 ms	69.9 ± 22 ms